Journal of Dental Sciences 20 (2025) 1422–1435

Available online at www.sciencedirect.com

ScienceDirect

journal homepage: www.e-jds.com

Original Article

Micro-/nano-structured zirconia surface promotes osteogenic differentiation of human bone marrow mesenchymal stem cells by reducing pyroptosis under inflammatory conditions

Hui-Min Wang †, Qian Ding †, Ying Chen, Yao-Jun Zhang, Zhi-Xiao Wu, Xiao Zhang *, Lei Zhang **

Department of Prosthodontics, Peking University School and Hospital of Stomatology & National Center of Stomatology & National Clinical Research Center for Oral Diseases & National Engineering Laboratory for Digital and Material Technology of Stomatology & Beijing Key Laboratory of Digital Stomatology & Research Center of Engineering and Technology for Computerized Dentistry Ministry of Health & NMPA Key Laboratory for Dental Materials, Beijing, China

Received 19 January 2025; Final revision received 11 February 2025
Available online 20 February 2025

KEYWORDS
Cell pyroptosis;
hBMSCs;
Inflammatory conditions;
Micro-/nano-structured zirconia surface;
Osteogenic differentiation

Abstract *Background/purpose:* Promoting osteogenesis under inflammatory conditions holds promise for preventing and mitigating peri-implantitis. Cell pyroptosis inhibits osteoblast-mediated bone formation. Although the surface topography of implant materials influences both osteogenesis and inflammatory responses, its effects on pyroptosis and osteogenesis under inflammatory conditions have not been thoroughly investigated. The aim of this study was to investigate the effects of a porous and hydrofluoric acid-etched micro-/nano-structured zirconia (POROHF) surface on pyroptosis and osteogenesis of human bone marrow mesenchymal stem cells (hBMSCs) under inflammatory conditions.

Materials and methods: Lipopolysaccharide (LPS) and adenosine 5′-triphosphate (ATP) were used to induce pyroptosis in hBMSCs and evaluate the effects of pyroptosis on osteogenesis of hBMSCs. Then, using commonly used sandblasted acid-etched titanium and zirconia surfaces as controls, the effects of POROHF surface on pyroptosis and osteogenesis under inflammatory conditions simulated by LPS and ATP were evaluated. To clarify the potential mechanisms by

* Corresponding author. Department of Prosthodontics, Peking University School and Hospital of Stomatology, 22 Zhongguancun Avenue South, Haidian District, Beijing 100081, China.
** Corresponding author. Department of Prosthodontics, Peking University School and Hospital of Stomatology, 22 Zhongguancun Avenue South, Haidian District, Beijing 100081, China.
E-mail addresses: kqxiaozhang@hsc.pku.edu.cn (X. Zhang), drzhanglei@yeah.net (L. Zhang).
† Both authors contributed equally to this study.

https://doi.org/10.1016/j.jds.2025.02.012

which the surface affected pyroptosis of hBMSCs, RNA sequencing and functional verification were also performed.
Results: LPS and ATP induced caspase-1/GSDMD-mediated pyroptosis in hBMSCs and thereby inhibited osteogenic differentiation and angiogenic potential of hBMSCs, which could be partially reversed by inhibiting pyroptosis. The POROHF surface could reduce pyroptosis levels, thereby promoting osteogenesis of hBMSCs under inflammatory conditions. The surface reduced pyroptosis of hBMSCs by downregulating *EGR1* expression and upregulating *MANF* expression.
Conclusion: This study highlighted the inhibitory effects of caspase-1/GSDMD-mediated pyroptosis on osteogenesis of hBMSCs and demonstrated that micro-/nano-structured zirconia surface could promote osteogenic differentiation of hBMSCs by reducing pyroptosis under inflammatory conditions.

Introduction

Peri-implantitis is a common biological complication of implant therapy that is characterized by inflammation of the peri-implant tissues and continuous resorption of the supporting bone tissues, which can ultimately result in implant failure.[1] It affects approximately 19.5 % of patients and 12.5 % of implants.[2] However, specific treatments for peri-implantitis remain unavailable. Considering its pathogenesis, mitigating the inflammatory responses in peri-implant tissues, inhibiting the resorption of supporting bone tissues, and promoting osteogenesis under inflammatory conditions hold promise for the management and prevention of peri-implantitis.[3]

Pyroptosis is a pro-inflammatory form of programmed cell death mediated primarily by caspases and gasdermin.[4] The canonical pathway of pyroptosis is triggered by the activation of inflammasomes such as NLR family pyrin domain containing 3 (NLRP3), which further activate caspase-1. Activated caspase-1 cleaves both gasdermin D (GSDMD) and the precursors of interleukin-18 (IL-18) and IL-1β.[5] The cleaved N-terminal fragment of GSDMD (GSDMD-N) forms transmembrane pores, thereby initiating pyroptosis, releasing substantial amounts of cellular contents, and activating robust inflammatory responses.[5] Aberrant activation of pyroptosis can inhibit osteoblast-mediated bone formation, leading to an imbalance in bone metabolism.[5] Recent researches have revealed the significant effects of pyroptosis on the inflammatory bone loss observed in conditions such as apical periodontitis, rheumatoid arthritis, and periodontitis.[6] Additionally, increased expression of pyroptosis-associated factors has been detected in inflamed tissues surrounding peri-implantitis lesions.[7,8] Considering these findings, targeting pyroptosis represents a promising strategy for reducing the bone loss associated with peri-implantitis.

In recent decades, titanium has become the predominant material employed in dental implants. Among commercially available options, sandblasted, large-grit, and acid-etched surface is recognized as standard choice for titanium implants.[9] Meanwhile, zirconia has gained attention as a promising alternative to titanium for its outstanding physical and mechanical performance, enhanced biocompatibility, and better aesthetic performance.[10] Notably, zirconia exhibits a low attraction to bacterial plaque biofilms and is associated with reduced inflammatory responses compared to titanium.[11] Researches have shown that hierarchical structures combining micro- and nano-topographic features on implant material surfaces can enhance osteogenic performance while reducing inflammatory responses.[12,13] Nevertheless, few researches have revealed the effects of different surface topographies on pyroptosis levels and osteogenic performance under inflammatory conditions. Our research group has previously developed a micro-/nano-structured zirconia surface and confirmed its excellent osteogenic performance under physiological conditions.[14] However, it remains uncertain how it performs under inflammatory conditions.

Therefore, the aim of this study was to investigate the effects and relevant mechanisms of the micro-/nano-structured zirconia surface on pyroptosis levels and osteogenic differentiation of human bone marrow mesenchymal stem cells (hBMSCs) under inflammatory conditions, using commonly used sandblasted acid-etched titanium and zirconia surfaces as controls.

Materials and methods

Titanium and zirconia specimen preparation

The specimens used in this study were divided into the following groups based on the materials and treatment methods:

Sandblasted, large-grit, and acid-etched titanium (SLA): Commercial titanium specimens (Chengdu Xin Hang Feng Technology Co., Ltd., Chengdu, China) were sandblasted with 250-μm alumina particles, followed by acid etching with a 1:1 (v/v) solution of 10 % H_2SO_4 and 10 % HCl at 60 °C for 30 min.

Sandblasted and hydrofluoric acid-etched zirconia (SBHF): Zirconia specimens (Wieland Dental, Pforzheim, Germany) were sandblasted with 110-μm alumina particles and etched at room temperature using 40 % hydrofluoric acid for 60 min.

Porous and hydrofluoric acid-etched zirconia (POROHF): The source and preparation methods for these specimens were consistent with those described in our previous research.[14] The porous surface zirconia specimens were manufactured using a dry-pressing technique that

incorporated pore formers. They were subsequently etched with 40 % hydrofluoric acid for 60 min. Residual acid was first rinsed away by running water and then cleaned with high-pressure air. Finally, the specimens were ultrasonically cleaned twice for 20 min in deionized water.

Subsequently, all specimens underwent ultrasonic cleaning for 30 min each with acetone, anhydrous ethanol, and deionized water. The specimens were dried in the air. For cell culture experiments, the specimens underwent sterilization in an autoclave at 121.3 °C for 30 min.

Titanium and zirconia specimen characterization

The surface morphologies of the disc-shaped titanium and zirconia specimens (15 mm in diameter, 1 mm in thickness) were observed using a three-dimensional (3D) laser microscope (VK-X200; Keyence Co., Osaka, Japan). The pore size of the POROHF surface and surface roughness of all specimens were analyzed using the accompanying software (VK Analyzer; Keyence Co.). A field emission scanning electron microscope (FESEM; SU8010; Hitachi, Tokyo, Japan) was applied to further observe surface topographies, and the surface elemental composition was examined with an energy dispersive spectrometer (EDS). Surface wettability was evaluated by analyzing the static contact angle with a contact angle goniometer (OCA50; DataPhysics, Filderstadt, Germany). Additionally, the crystalline phase composition was analyzed with X-ray diffraction (XRD; D8 Advance; Bruker, Karlsruhe, Germany). The intensity ratios of monoclinic peaks and the volumes of monoclinic phase in the zirconia specimens were calculated using formulas described in previous literature.[15,16]

Cell culture and induction of pyroptosis under inflammatory conditions

Cells were obtained from Procell Life company (Procell Life Science and Technology Co., Ltd., Wuhan, China). They were cultured in a complete medium composed of alpha minimal essential medium, 1 % (v/v) penicillin/streptomycin, and 10 % (v/v) fetal bovine serum (Thermo Fisher Scientific, Waltham, MA, USA). For the experiments, hBMSCs at passages 3—7 were applied.

To induce pyroptosis in hBMSCs, initial cell experiments were conducted on blank plates without specimens. Based on previous researches and pilot experiments,[17,18] 1 μg/mL lipopolysaccharide (LPS; InvivoGen, San Diego, CA, USA) and 5 mM adenosine 5′-triphosphate (ATP; MedChemExpress, Monmouth Junction, NJ, USA) were simultaneously added to medium to simulate inflammatory conditions. Cells cultured in normal medium were designated as the control group. To confirm the presence of pyroptosis, hBMSCs were plated into blank 24-well plates at 7.5×10^4 cells per well. After 8 h of LPS and ATP treatments, pyroptotic morphology was observed using a light microscope (BX51M; Olympus, Tokyo, Japan).

Reverse transcription quantitative polymerase chain reaction

Cells were plated into blank 24-well plates at 7.5×10^4 cells per well. To elucidate the signaling pathway of pyroptosis in hBMSCs, the mRNA expression levels of pyroptosis-associated genes were first determined in the control and inflammatory stimulation groups. After confirming that LPS and ATP could induce caspase-1/GSDMD-mediated pyroptosis in hBMSCs, a caspase-1 inhibitor, VX-765 (Abmole Bioscience, Houston, TX, USA), was included in subsequent experiments.[19] Therefore, cell experiments conducted on blank plates included a control group (Control), an inflammatory stimulation group (LPS + ATP), and an inhibitor group (LPS + ATP + VX-765) in which cells were pretreated with 10 μM VX-765 for 60 min before LPS and ATP treatments. Based on the pyroptotic morphology observed after 8 h of LPS and ATP treatments, pyroptosis-associated gene levels were determined at the same time point. In addition, to compare the pyroptosis levels of hBMSCs on different surfaces, hBMSCs were plated onto three groups of specimens (15 mm in diameter, 1 mm in thickness) placed in 24-well plates and subjected to LPS and ATP treatments for 8 h to determine pyroptosis-associated gene levels.

To assess the regulatory effects of pyroptosis on the osteogenic differentiation and angiogenic potential of hBMSCs, hBMSCs from the three groups on blank plates underwent 2 weeks of osteogenic induction. For the LPS + ATP group and LPS + ATP + VX-765 group, drug treatments were administered during the first week. The osteogenic induction medium for all groups was supplemented with 50 μg/mL L-ascorbic acid, 10 mM β-glycerophosphate, and 100 nM dexamethasone (all from Sigma—Aldrich, St. Louis, MO, USA). To assess the regulatory effects of pyroptosis on osteogenic differentiation and angiogenic potential of hBMSCs on different surfaces under inflammatory conditions, hBMSCs were plated onto three groups of specimens in 24-well plates and subjected to 2 weeks of osteogenic induction. During the first week, hBMSCs were subjected to LPS and ATP treatments, with or without VX-765 pretreatment. Total RNA was collected to quantify the mRNA levels of osteogenic- and angiogenic-associated genes.

Total RNA was collected with AG RNAex Pro reagent (Accurate Biotechnology (Hunan) Co., Ltd, Changsha, China). After conversion to complementary DNAs (cDNAs), reverse transcription quantitative polymerase chain reaction (RT-qPCR) was conducted on ABI 7500 PCR System (Applied Biosystems, Foster City, CA, USA). The sequences utilized in the experiments were listed in Table S1, with *GAPDH* as reference gene.

Western blot detection of pyroptosis-associated proteins

Cells were plated into blank 6-well plates at 5×10^5 cells per well and subjected to drug treatments for 24 h. To confirm the presence of pyroptosis and identify the underlying signaling pathway, the protein levels of caspase-1, -4, -5, cleaved caspase-1, and GSDMD-N were initially assessed in the Control and LPS + ATP groups. Following confirmation that LPS and ATP induced caspase-1/GSDMD-mediated pyroptosis in hBMSCs, the effects of VX-765 on pyroptosis-associated protein levels were assessed to further validate the signaling pathway. To compare

pyroptosis levels of hBMSCs on different surfaces, hBMSCs were plated onto titanium and zirconia specimens (35 mm in diameter, 1 mm in thickness) placed in 6-well plates and subjected to LPS and ATP treatments for 24 h.

Cells were lysed using RIPA buffer (Solarbio, Beijing, China) containing phenylmethylsulphonyl fluoride (Solarbio). After determining protein concentrations with a bicinchoninic acid (BCA) kit (EpiZyme, Shanghai, China), equal quantities of proteins were separated by SDS gel electrophoresis, transferred to PVDF membranes, and blocked using blocking buffer (EpiZyme). The membranes were incubated with the following primary antibodies for 12 h at 4 °C: cleaved caspase-1 (#4199; Cell Signaling Technology, Danvers, MA, USA), caspase-1 (ab207802; Abcam, Cambridge, UK), cleaved GSDMD (#36425; Cell Signaling Technology), GSDMD (ab210070; Abcam), caspase-4 (11856-1-AP; Proteintech, Chicago, IL, USA), caspase-5 (ab40887; Abcam), and GAPDH (TA-08; ZSGB-Bio, Beijing, China). After incubation with the appropriate secondary antibodies, protein bands were visualized based on chemiluminescence reagent (P1050; Applygen Technologies, Beijing, China).

Enzyme-linked immunosorbent assay

Cells were plated into blank 6-well plates at 5×10^5 cells per well. The LPS + ATP and LPS + ATP + VX-765 groups were treated with the respective drugs for 24 h. Additionally, hBMSCs were plated onto titanium and zirconia specimens in 6-well plates and subjected to LPS and ATP treatments for 24 h. The cell supernatants were collected, and IL-18 and IL-1β secretion levels were assessed with enzyme-linked immunosorbent assay (ELISA) kits (Solarbio) based on the instructions.

Flow cytometric analysis

Cells were plated into blank 6-well plates at 5×10^5 cells per well. The LPS + ATP group was treated with LPS and ATP for 24 h and the LPS + ATP + VX-765 group was pretreated with 10 μM VX-765 for 60 min before LPS and ATP treatments for 24 h. Then hBMSCs were collected, washed, and suspended. Subsequently, hBMSCs were incubated with propidium iodide (PI) and fluorescein isothiocyanate (FITC)-labeled annexin V (Annexin V-FITC) staining solution (both from BD Biosciences, Franklin Lakes, NJ, USA). The cells were then analyzed with a flow cytometer (BD Biosciences). Cells which were double positive for Annexin V-FITC/PI were identified as pyroptotic cells.

Cell morphology on different surfaces under inflammatory conditions

Cells were plated onto three groups of specimens in a 24-well plate at 2×10^4 cells per well and subjected to LPS and ATP treatments for 8 h and 24 h. After fixation and permeabilization, hBMSCs were treated with FITC-conjugated phalloidin (Solarbio) and 4',6-diamidino-2-phenylindole (Sigma—Aldrich). The stained specimens were then visualized using a confocal microscope (LSM710; Zeiss, Oberkochen, Germany).

Cell proliferation on different surfaces under inflammatory conditions

Cells were plated onto three groups of specimens (10 mm in diameter, 1 mm in thickness) in 48-well plates at 2×10^4 cells per well. After attachment, hBMSCs were subjected to LPS and ATP treatments for 1, 3, 5, and 7 days, respectively. Next, the cells were treated with cell counting kit-8 (CCK8; Beyotime, Shanghai, China) for 2.5 h. A microplate reader (Multiskan Sky; Thermo Fisher Scientific) was used to read the optical density at 450 nm.

Staining and quantitative assessment of alkaline phosphatase and alizarin red S

To assess alkaline phosphatase (ALP) activity, hBMSCs were divided into Control, LPS + ATP, and LPS + ATP + VX-765 groups and then underwent osteogenic induction for 1 week. During this period, the LPS + ATP group was treated with LPS and ATP, while the LPS + ATP + VX-765 group received pretreatment with VX-765 followed by LPS and ATP treatments. Additionally, hBMSCs were plated onto three groups of specimens in 24-well plates at 5×10^4 cells per well and then subjected to osteogenic induction and LPS and ATP treatments for 1 week, with or without VX-765 pretreatment. ALP staining was conducted with an ALP staining kit (Beyotime). ALP activity was quantified with an ALP activity kit (Nanjing Jiancheng Bioengineering Institute, Nanjing, China), while the protein content was quantified with a BCA kit.

To assess the mineralization levels of the extracellular matrix (ECM), hBMSCs from the above groups were incubated for 3 weeks in osteogenic induction medium. During the first week, the LPS + ATP group was treated with LPS and ATP, while the LPS + ATP + VX-765 group underwent pretreatment with VX-765 followed by LPS and ATP treatments. Alizarin red S (ARS) staining was performed using an ARS solution (Solarbio). To quantify the mineralization levels of ECM, the ARS-stained calcium deposits were dissolved in 10 % (w/v) cetylpyridinium chloride solution (Sigma—Aldrich) for 30 min at room temperature. The absorbance of the resulting solution was measured at 562 nm using a microplate reader (Multiskan Sky; Thermo Fisher Scientific).

RNA sequencing and functional verification

To explore the potential mechanisms by which the POROHF surface affected pyroptosis of hBMSCs, RNA sequencing was performed.[20] Cells were plated onto titanium and zirconia specimens in 24-well plates with five replicates per group, and RNA was collected after LPS and ATP treatments for 8 h. Double-stranded cDNAs were synthesized for library construction and subsequent quality control. Sequencing was conducted on the Illumina NovaSeq 6000 platform. The raw reads were aligned to the GRCh38. Gene levels were determined using the subread software. The DESeq2 package was then applied to detect differentially expressed genes (DEGs). The DEGs were then analyzed for Gene Ontology enrichment. Images depicting the analysis were generated using the ggplot2 package in R. The selected DEGs were further validated through RT-qPCR. Genes with significant

differences and consistent with the RNA sequencing results were selected as key DEGs, including early growth response 1 (*EGR1*) and mesencephalic astrocyte derived neurotrophic factor (*MANF*). To further verify the function of key DEGs, *EGR1* and *MANF* of hBMSCs plated on POROHF specimens were silenced by using corresponding small interfering RNA (siRNA) and transfection reagent (GenePharma, Shanghai, China). The sequences were listed in Table S2. The groups in this experiment included *EGR1*-siRNA group (hBMSCs transfected with *EGR1*-siRNA sequences), *MANF*-siRNA group (hBMSCs transfected with *MANF*-siRNA sequences), and negative control (NC) group (hBMSCs transfected with NC-siRNA sequences). After transfection and stimulation with LPS and ATP for 8 h, RNA was collected to determine pyroptosis-associated gene levels.

Statistical analysis

All above experiments were conducted in triplicate unless explicitly stated otherwise. Results were expressed as means ± standard deviation (SD). SPSS 26.0 software (IBM Corp., Armonk, NY, USA) was used for data analysis. Student's t-test was applied to assess differences between two groups, whereas one-way analysis of variance was applied to assess differences among multiple groups. For post hoc analysis, the least significant difference test was applied for multiple groups with equal variances, while the Games—Howell test was applied for multiple groups with unequal variances. *P*-value <0.05 was deemed statistically significant.

Results

Titanium and zirconia specimen characterization

The micro-/nano-structured zirconia surfaces were successfully fabricated by acid etching porous surface zirconia specimens, as previously described.[14] As illustrated in the 3D reconstruction of surface morphologies (Fig. 1A), the POROHF specimens displayed densely packed pore structures with rough inter-pore regions, whereas the SBHF and SLA specimens exhibited uneven, rough surfaces. The measured pore size of the POROHF specimens was 232.33 ± 22.13 μm. FESEM (Fig. 1B) revealed that the POROHF specimens possessed uniformly distributed micron-scale pore structures with irregularly shaped nano-scale particles on their inner walls, 50—500 nm in diameter. Conversely, the SLA specimens featured a network-like rough surface with numerous micro-scale pits, whereas the SBHF specimens displayed an irregular groove-ridge structure composed of nano-scale particles.

EDS analysis indicated that titanium was the primary element in the SLA specimens, while zirconium and oxygen were the main elements in the SBHF and POROHF specimens, with no impurities detected (Fig. 1C). The roughness between the pores of the POROHF specimens was significantly lower than that of the SLA and SBHF specimens (Fig. 1D). The POROHF specimens also exhibited a significantly lower contact angle compared to the SLA and SBHF specimens, highlighting their enhanced hydrophilicity (Fig. 1E and F). XRD analysis (Fig. 1G) of the SLA specimens revealed prominent peaks corresponding to pure titanium, along with a minor presence of titanium hydride. The POROHF specimens showed no distinct peaks related to the monoclinic phase, which accounted for only 3.33 % of their composition. Conversely, the SBHF specimens exhibited a pronounced peak associated with the monoclinic phase, comprising 9.21 % of their composition.

LPS and ATP induced caspase-1/GSDMD-mediated pyroptosis in hBMSCs

To induce pyroptosis in hBMSCs, LPS and ATP were used to simulate inflammatory conditions and administered simultaneously to enhance stimulation intensity. After 8 h of LPS and ATP treatments, hBMSCs exhibited swelling, with some cells exhibiting morphological characteristics typical of pyroptosis such as ruptured membranes and cytoplasmic blebbing (Fig. 2A). Meanwhile, the mRNA expression levels of pyroptosis-associated factors, including *NLRP3*, *caspase-1*, *caspase-5*, and *GSDMD*, were significantly increased, whereas *caspase*-4 mRNA levels showed minimal changes (Fig. 2C). After 24 h, caspase-1 protein levels were significantly increased, with prominent cleaved bands observed for both caspase-1 and GSDMD. However, the caspase-5 and caspase-4 protein levels showed minimal changes (Fig. 2B). These results implied that LPS and ATP induced caspase-1/GSDMD-mediated pyroptosis in hBMSCs. To verify the involvement of this pathway, caspase-1 inhibitor VX-765 was introduced in subsequent experiments.[19] VX-765 partially reversed the LPS- and ATP-induced increases in mRNA and protein levels of both caspase-1 and GSDMD, and the appearance of cleaved bands for both proteins (Fig. 2D—F). Furthermore, the increased mRNA and secretion levels of IL-18 and IL-1β were also partially reversed by VX-765 (Fig. 2D—G). Flow cytometric analysis revealed a significant increase in Annexin V-FITC/PI double-positive cells, indicative of pyroptosis, following LPS and ATP treatment. VX-765 pretreatment partially reversed this increase (Fig. 2E). In summary, LPS and ATP induced caspase-1/GSDMD-mediated pyroptosis in hBMSCs, which could be effectively inhibited by VX-765.

Caspase-1/GSDMD-mediated pyroptosis inhibited osteogenic differentiation and angiogenic potential of hBMSCs

The osteogenic- and angiogenic-associated gene levels (*ALP*, *BMP2*, *Collagen 1*, *RUNX2*, *ANGPT1*, and *VEGFB*) were significantly decreased after LPS and ATP treatments (Fig. 3A). Furthermore, ALP activity was markedly inhibited, as demonstrated by ALP staining and quantitative assessment (Fig. 3B and C). Similarly, ECM mineralization levels were decreased, as shown by ARS staining and quantitative assessment (Fig. 3D and E). Notably, these inhibitory effects were reversed by pretreatment with VX-765. These findings indicated that caspase-1/GSDMD-mediated pyroptosis inhibited both osteogenic differentiation and angiogenic potential of hBMSCs. Pretreatment with VX-765 effectively reduced pyroptosis levels, thereby promoting osteogenic differentiation and angiogenic potential of hBMSCs under inflammatory conditions.

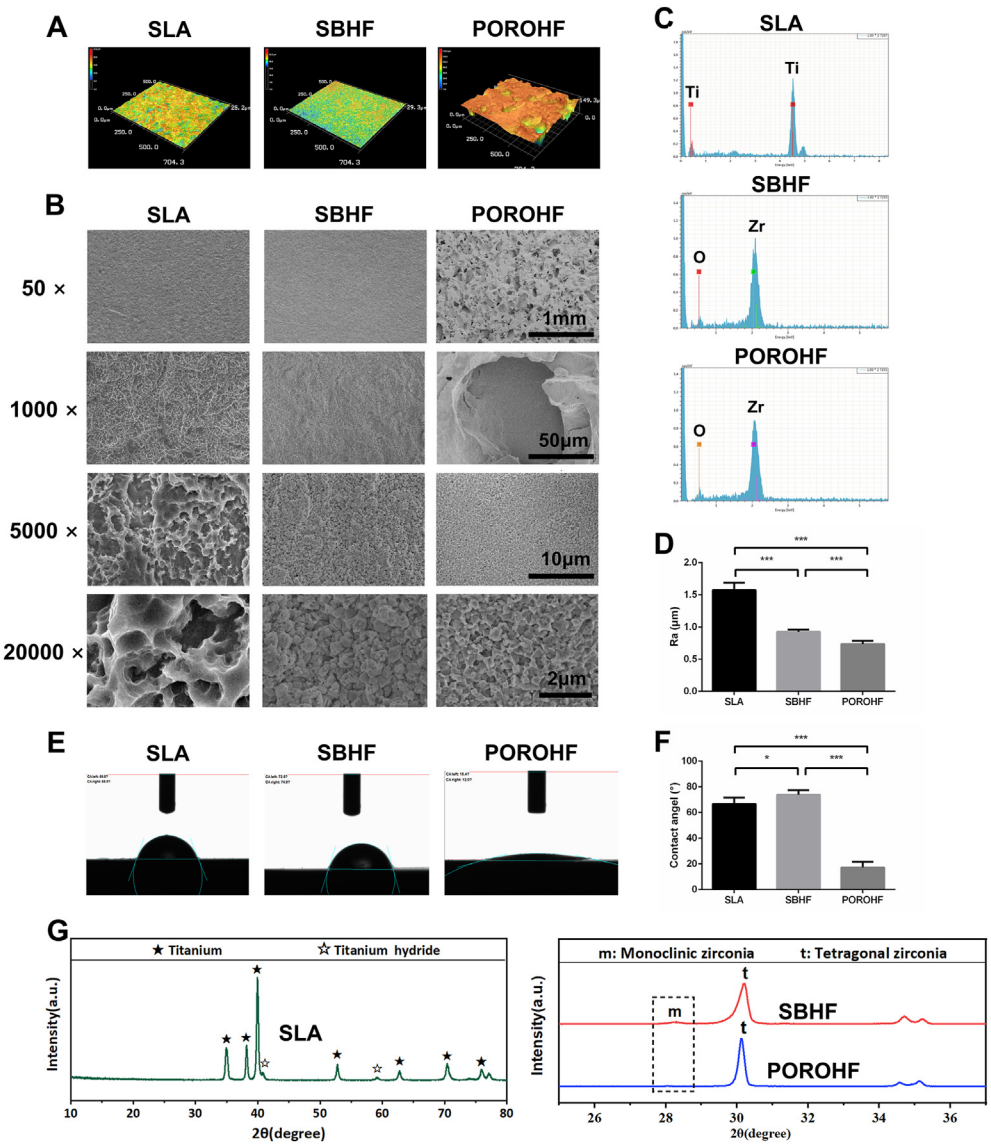

Figure 1 Titanium and zirconia specimen characterization. (A) Three-dimensional (3D) morphologies of the specimen surfaces. (B) Field emission scanning electron microscope (FESEM) images of surface topographies at magnifications of 50 × , 1,000 × , 5,000 × , and 20,000 × . (C) Energy dispersive spectrometer (EDS) analysis of the elemental composition. (D) Surface roughness analysis. (E, F) Static contact angle analysis for surface wettability. (G) X-ray diffraction (XRD) analysis of the crystalline phase composition. Results are expressed as means ± SD, n = 10. *$P < 0.05$, ***$P < 0.001$. a.u.: arbitrary unit, CA: contact angel, m: monoclinic zirconia, O:oxygen, POROHF: porous and hydrofluoric acid-etched zirconia, Ra: arithmetic average roughness, SBHF: sandblasted and hydrofluoric acid-etched zirconia, SLA: sandblasted, large-grit, and acid-etched titanium, t: tetragonal zirconia, Ti: titanium, Zr: zirconium.

Micro-/nano-structured zirconia surface reduced pyroptosis and was beneficial for hBMSC adhesion and proliferation under inflammatory conditions

The mRNA expression levels of pyroptosis-associated factors were significantly lower on the zirconia surfaces than on the SLA surface under inflammatory conditions. Notably, the mRNA expression levels of *NLRP3* and *IL-18* were significantly reduced on the POROHF surface compared to the SBHF surface (Fig. 4A). The protein expression levels of caspase-1, GSDMD, cleaved caspase-1, and GSDMD-N (Fig. 4B), and the secretion levels of IL-18 and IL-1β (Fig. 4C), on the zirconia surfaces were lower than those on the SLA surface. Among the zirconia surfaces, the levels of these proteins on the POROHF surface were lower than those on the SBHF surface.

As shown in Fig. 4D, hBMSCs exhibited an elongated spindle shape after 8 h of exposure to inflammatory conditions, with numerous filopodia and lamellipodia extending on the POROHF surface. Conversely, cells on the SLA and SBHF surfaces formed several lamellipodia. After 24 h of exposure, hBMSCs on the POROHF surface adopted a polygonal shape, extending in multiple directions, whereas cells on the SLA and SBHF surfaces became more elongated.

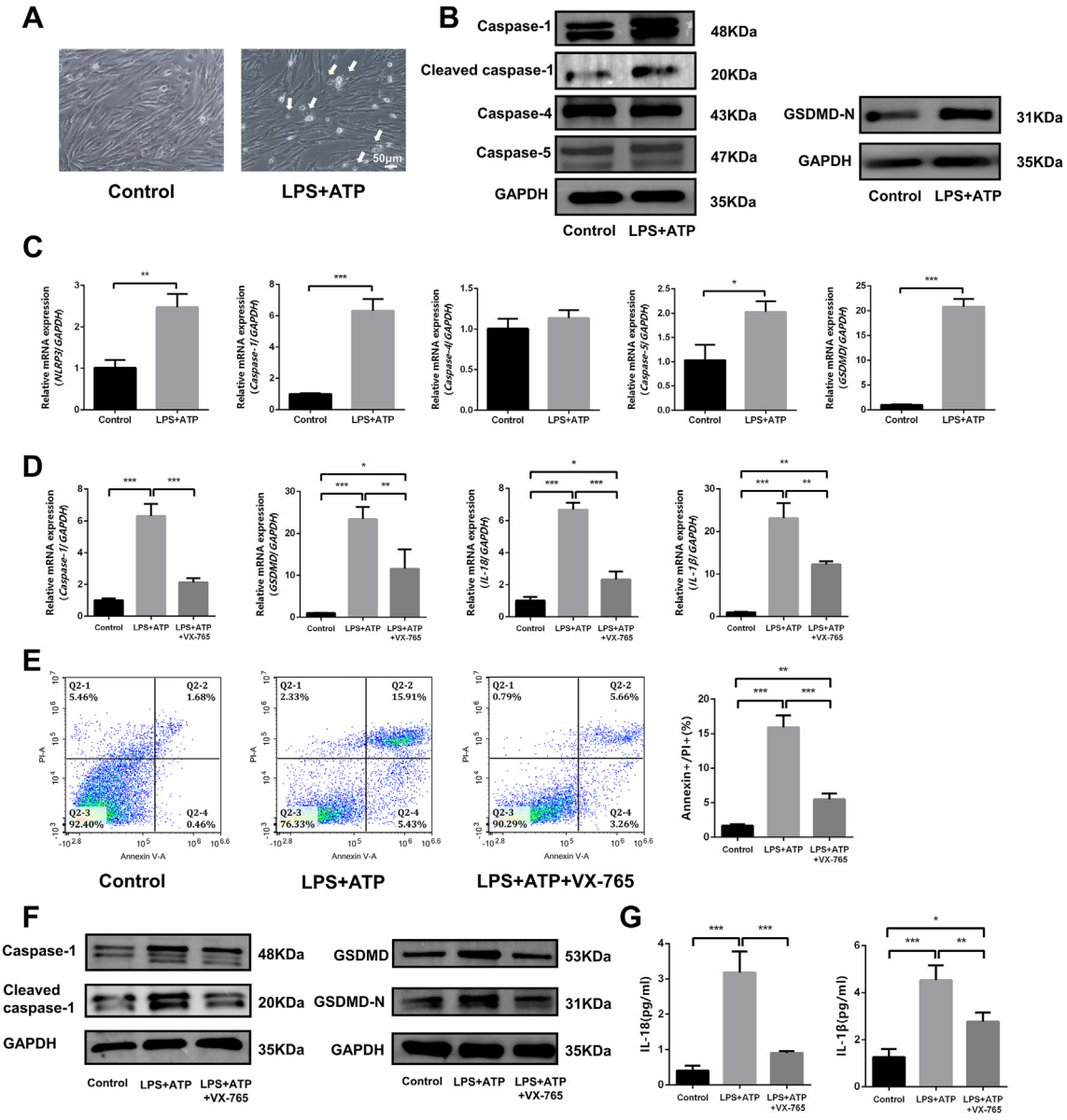

Figure 2 Caspase-1/GSDMD-mediated pyroptosis in human bone marrow mesenchymal stem cells (hBMSCs) induced by LPS and ATP. (A) Morphological observation of pyroptosis. White arrows indicate pyroptotic cells. (B) Western blot detection of pyroptosis-associated proteins after 24 h of LPS and ATP treatments. (C) Pyroptosis-associated gene levels after 8 h of LPS and ATP treatments. (D) Pyroptosis-associated gene levels in the Control, LPS + ATP, and LPS + ATP + VX-765 groups. (E) Flow cytometric analysis of fluorescein isothiocyanate-labeled annexin V (Annexin V-FITC)/PI staining in the above three groups. (F) Western blot detection of pyroptosis-associated proteins in the above three groups. (G) IL-18 and IL-1β secretion levels in the above three groups. Results are expressed as means ± SD, n = 3. $^{*}P < 0.05$, $^{**}P < 0.01$, $^{***}P < 0.001$. ATP: adenosine 5′-triphosphate, GAPDH: glyceraldehyde-3-phosphate dehydrogenase, GSDMD: gasdermin D, GSDMD-N: N-terminal fragment of GSDMD, IL: interleukin, LPS: lipopolysaccharide, NLRP3: NLR family pyrin domain containing 3, PI: propidium iodide.

3D scanning and reconstruction of hBMSCs adhered to the POROHF surface revealed that some cells stretched into the pores, extending toward the edges and bases of the pore structures (Fig. S1).

As shown in Fig. 4E, the proliferation levels of hBMSCs were comparable among all groups at 1 and 3 days. However, at 5 and 7 days, the proliferation levels of hBMSCs were significantly higher on the POROHF surface than on the SBHF and SLA surfaces.

The results indicated that under inflammatory conditions, zirconia surfaces exhibited reduced expression levels of pyroptosis-associated factors compared to the SLA surface, with the POROHF surface demonstrating the lowest expression levels. Furthermore, under inflammatory

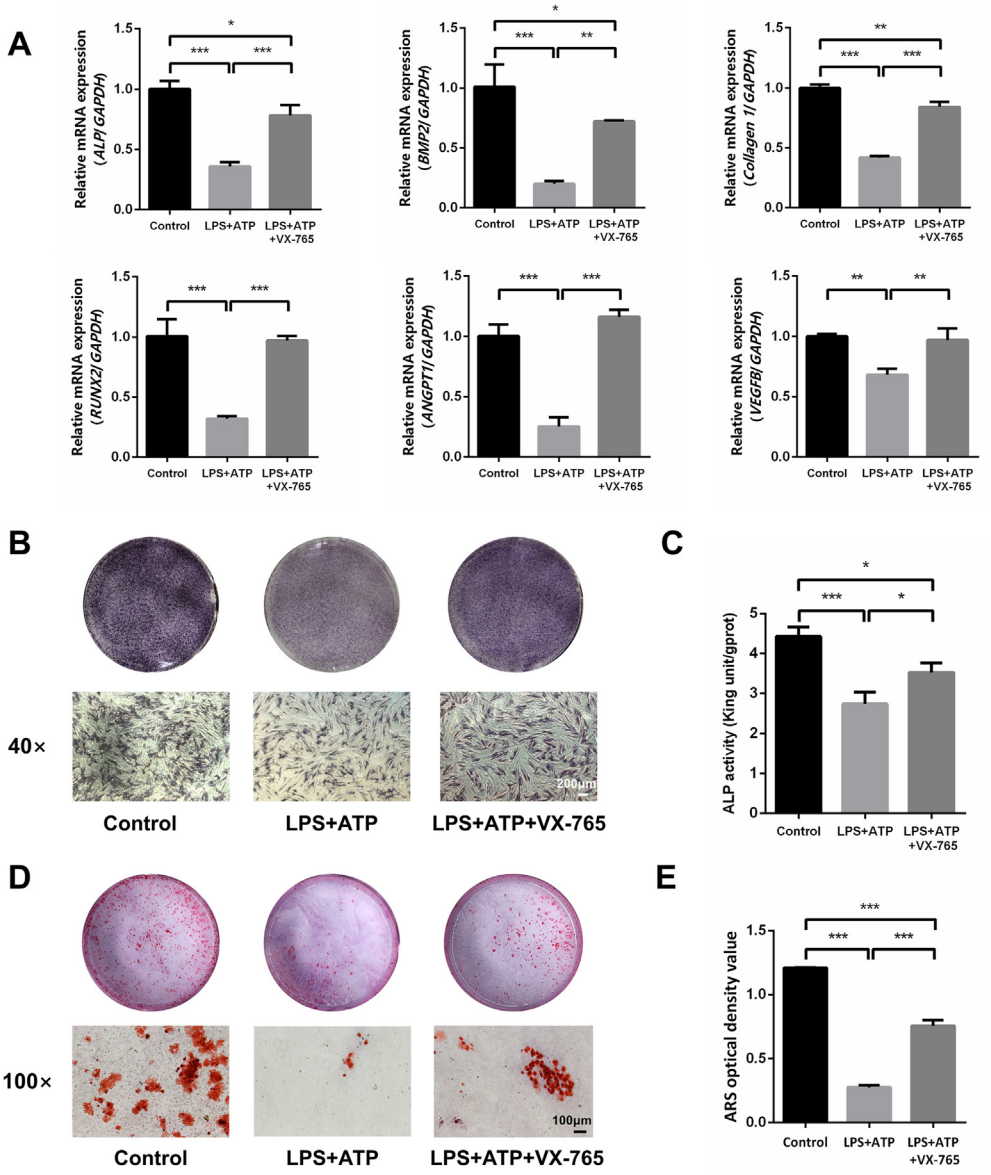

Figure 3 Effects of pyroptosis on osteogenic differentiation and angiogenic potential of human bone marrow mesenchymal stem cells (hBMSCs). (A) Osteogenic- and angiogenic-associated gene levels. (B, C) ALP staining at magnifications of 1 × and 40 × and quantitative assessment of ALP activity. (D, E) ARS staining at magnifications of 1 × and 100 × and quantitative assessment of extracellular matrix (ECM) mineralization levels. Results are expressed as means ± SD, n = 3. *$P < 0.05$, **$P < 0.01$, ***$P < 0.001$. ALP: alkaline phosphatase, ANGPT1: angiopoietin 1, ARS: Alizarin red S, ATP: adenosine 5′-triphosphate, BMP2: bone morphogenetic protein 2, GAPDH: glyceraldehyde-3-phosphate dehydrogenase, gprot: gram protein, LPS: lipopolysaccharide, RUNX2: RUNX family transcription factor 2, VEGFB: vascular endothelial growth factor B.

conditions, the POROHF surface promoted hBMSC adhesion and proliferation.

Micro-/nano-structured zirconia surface promoted osteogenic differentiation and angiogenic potential of hBMSCs, and inhibiting pyroptosis could enhance osteogenic performance of the material surfaces

As shown in Fig. 5A, the POROHF surface exhibited significantly higher expression levels of osteogenic-associated genes (*ALP*, *BMP2*, *Collagen 1*, *RUNX2*) and angiogenic-associated genes (*ANGPT1*, *VEGFB*) compared to the SLA and SBHF surfaces under LPS and ATP treatments. With VX-765 pretreatment, mRNA expression levels in all groups increased significantly, with the POROHF surface maintaining the highest expression levels of both osteogenic- and angiogenic-associated genes. Due to the inherent color differences between the materials, with the SLA surface being gray (titanium) and the SBHF and POROHF surfaces being white (zirconia), the ALP and ARS staining results (Fig. 5B and D) could be visually influenced by the color of the materials. Therefore, quantitative analyses of ALP and ARS were performed to provide a more objective assessment of ALP activity and mineralization levels. The quantitative results

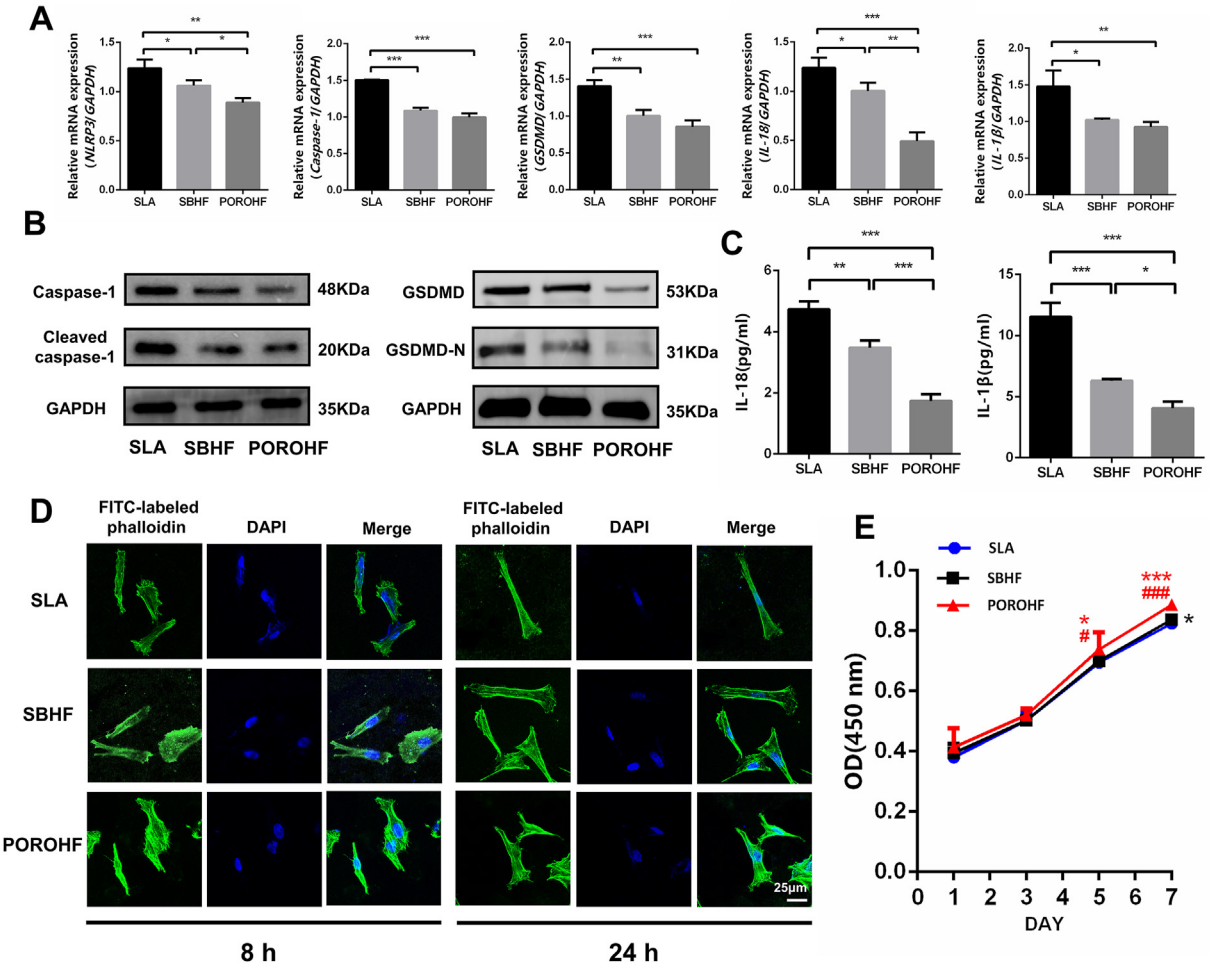

Figure 4 Effects of different surfaces on pyroptosis-associated factor expression, adhesion and proliferation of human bone marrow mesenchymal stem cells (hBMSCs) under inflammatory conditions. (A) Pyroptosis-associated gene levels. (B) Western blot detection of pyroptosis-associated proteins. (C) IL-18 and IL-1β secretion levels. (D) Adhesion of hBMSCs on different surfaces with inflammatory treatments for 8 and 24 h. Cytoskeletons were green, while nuclei were blue. (E) Proliferation of hBMSCs on different surfaces with inflammatory treatments for 1, 3, 5, and 7 days. $^{\#}$ and $^{\#\#\#}$ in Fig. E indicate significant differences in the proliferation of hBMSCs compared to the SBHF surface. * and *** in Fig. E indicate significant differences in the proliferation of hBMSCs compared to the SLA surface. Results are expressed as means ± SD, n = 3. *$P < 0.05$, **$P < 0.01$, ***$P < 0.001$, $^{\#}P < 0.05$, $^{\#\#\#}P < 0.001$. DAPI: 4′,6-diamidino-2-phenylindole, FITC: fluorescein isothiocyanate, GAPDH: glyceraldehyde-3-phosphate dehydrogenase, GSDMD: gasdermin D, GSDMD-N: N-terminal fragment of GSDMD, IL: interleukin, NLRP3: NLR family pyrin domain containing 3, OD: optical density, POROHF: porous and hydrofluoric acid-etched zirconia, SBHF: sandblasted and hydrofluoric acid-etched zirconia, SLA: sandblasted, large-grit, and acid-etched titanium.

(Fig. 5C and E) were consistent with the trends observed in the mRNA expression levels. These findings indicated that the POROHF surface promoted osteogenic differentiation and angiogenic potential of hBMSCs under inflammatory conditions. Moreover, inhibiting caspase-1/GSDMD-mediated pyroptosis with VX-765 could promote osteogenic differentiation and angiogenic potential of hBMSCs on the material surfaces under inflammatory conditions.

EGR1 and *MANF* were key DEGs that regulated pyroptosis levels of hBMSCs on the micro-/nano-structured zirconia surface

To clarify further the mechanisms by which the POROHF surface reduced pyroptosis and thereby promoted osteogenic differentiation of hBMSCs, DEGs were analyzed through RNA sequencing. To enrich more terms related to inflammation, a fold change <0.83 or >1.2 combined with $P < 0.05$ was used as the threshold for identifying DEGs.[21] 3,765 DEGs were identified between the POROHF and SLA groups, and 3,021 DEGs were identified between the POROHF and SBHF groups (Fig. 6A—C). Many DEGs were enriched in terms related to inflammation and adhesion, highlighted by the blue underlining (Fig. 6B—D). The selected DEGs, which might contribute to reducing pyroptosis levels in the POROHF group, were presented in the heatmap (Fig. 6E). RT-qPCR was used to further validate the mRNA levels of these selected DEGs (Fig. S2). Genes with significant differences and consistent with the RNA sequencing results were showed in Fig. 6F. Compared with

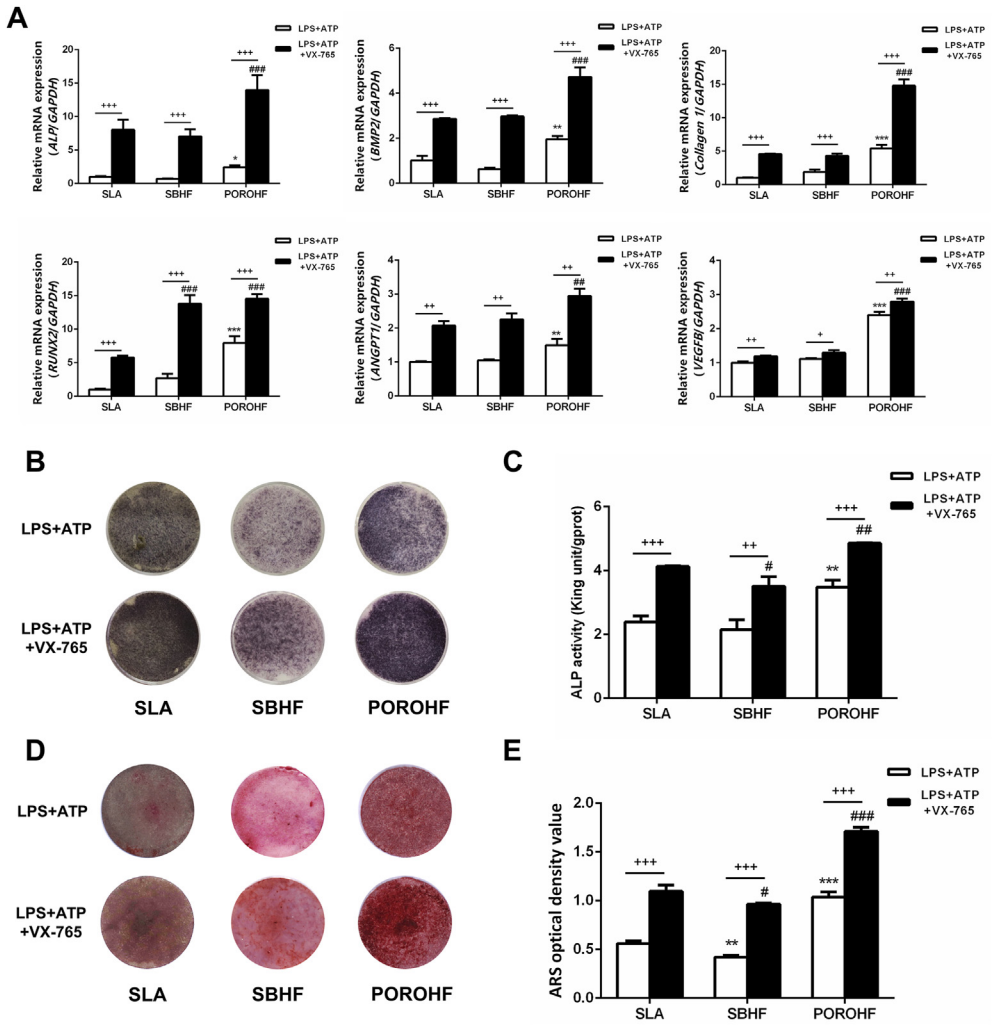

Figure 5 Osteogenic differentiation and angiogenic potential of human bone marrow mesenchymal stem cells (hBMSCs) under inflammatory conditions on different surfaces. (A) Osteogenic- and angiogenic-associated gene levels. (B, C) ALP staining and quantitative assessment of ALP activity. (D, E) ARS staining and quantitative assessment of extracellular matrix (ECM) mineralization levels. Results are expressed as means ± SD, n = 3. $^{*}P < 0.05$, $^{**}P < 0.01$, and $^{***}P < 0.001$ indicate significant differences compared to the LPS + ATP-SLA group. $^{\#}P < 0.05$, $^{\#\#}P < 0.01$, and $^{\#\#\#}P < 0.001$ indicate significant differences compared to the LPS + ATP + VX-765-SLA group. $^{+}P < 0.05$, $^{++}P < 0.01$, and $^{+++}P < 0.001$ indicate significant differences between the LPS + ATP and LPS + ATP + VX-765 groups on the same material surface. ALP: alkaline phosphatase, ANGPT1: angiopoietin 1, ARS: Alizarin red S, ATP: adenosine 5′-triphosphate, BMP2: bone morphogenetic protein 2, GAPDH: glyceraldehyde-3-phosphate dehydrogenase, gprot: gram protein, LPS: lipopolysaccharide, POROHF: porous and hydrofluoric acid-etched zirconia, RUNX2: RUNX family transcription factor 2, SBHF: sandblasted and hydrofluoric acid-etched zirconia, SLA: sandblasted, large-grit, and acid-etched titanium, VEGFB: vascular endothelial growth factor B.

the SLA and SBHF groups, the POROHF group exhibited significantly lower levels of *EGR1*, together with significantly higher levels of *MANF*. As shown in Fig. 7, the *EGR1*-siRNA group exhibited lower pyroptosis-associated gene levels (*NLRP3*,*GSDMD*,*caspase-1*,*IL-18*,and *IL-1β*) compared to the NC groups, while the *MANF*-siRNA group exhibited higher pyroptosis-associated gene levels compared to the NC group. Therefore, decreased expression of *EGR1* contributed to the reduction of pyroptosis, whereas decreased expression of *MANF* promoted pyroptosis. The downregulated expression of *EGR1* and upregulated expression of *MANF* on the POROHF surface contributed to the reduction of pyroptosis.

Discussion

Inadequate integration of peri-implant soft tissues can facilitate the invasion of Gram-negative bacteria. LPS, a virulence factor produced by Gram-negative bacteria, can activate the local inflammatory response.[3] Previous researches have revealed that LPS and ATP can induce pyroptosis in human gingival fibroblasts, macrophages, and osteoblasts.[22–24] To enhance stimulation intensity and induce pyroptosis in hBMSCs, LPS and ATP were selected as the inflammatory stimuli in this study. The results indicated that LPS and ATP induced caspase-1/GSDMD-mediated pyroptosis in hBMSCs, which inhibited both osteogenic

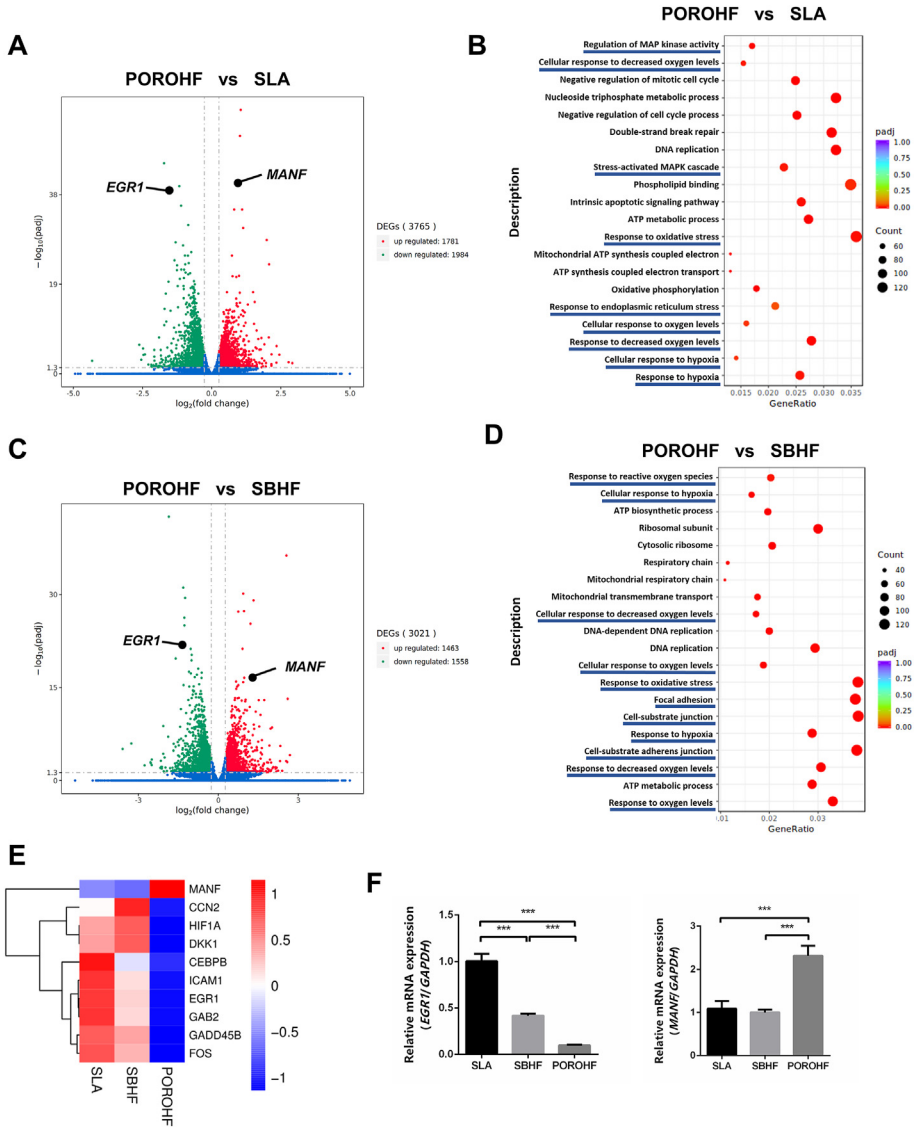

Figure 6 Differential gene expression analysis of human bone marrow mesenchymal stem cells (hBMSCs) on different surfaces. (A, C) Volcano plots displaying the distribution of differentially expressed genes (DEGs) between the POROHF and SLA/SBHF groups. Red dots represent significantly upregulated genes (POROHF vs. SLA/SBHF fold change >1.2, $P < 0.05$). Green dots represent significantly downregulated genes (SLA/SBHF vs. POROHF fold change >1.2, $P < 0.05$). Black dots represent key DEGs. (B, D) Scatter plots of Gene Ontology enrichment analysis for DEGs between the POROHF and SLA/SBHF groups. Terms underlined in blue represent selected terms associated with inflammation or adhesion. (E) Heatmap of selected DEGs. (F) Relative mRNA levels of key DEGs. Results are expressed as means ± SD, n = 3. ***$P < 0.001$. ATP: adenosine 5′-triphosphate, CCN2: cellular communication network factor 2, CEBPB: CCAAT enhancer binding protein beta, DKK1: dickkopf WNT signaling pathway inhibitor 1, EGR1: early growth response 1, FOS: Fos proto-oncogene, GAB2: GRB2 associated binding protein 2, GADD45B: growth arrest and DNA damage inducible beta, GAPDH: glyceraldehyde-3-phosphate dehydrogenase, HIF1A: hypoxia inducible factor 1 subunit alpha, ICAM1: intercellular adhesion molecule 1, MANF: mesencephalic astrocyte derived neurotrophic factor, MAP: mitogen-activated protein, MAPK: mitogen-activated protein kinase, POROHF: porous and hydrofluoric acid-etched zirconia, SBHF: sandblasted and hydrofluoric acid-etched zirconia, SLA: sandblasted, large-grit, and acid-etched titanium.

differentiation and angiogenic potential of hBMSCs. Pretreatment with caspase-1 inhibitor VX-765 effectively reduced pyroptosis levels, thereby promoting osteogenesis of hBMSCs. Consistent with these findings, previous researches have shown that pyroptosis inhibits osteoblast proliferation and differentiation, leading to impaired migration and osteogenic dysfunction.[5] Furthermore, the release of abundant of inflammatory factors, including IL-18 and IL-1β, as a result of pyroptosis, is responsible for the progression of bone loss.[25] Nevertheless, the specific signaling pathways through which pyroptosis inhibits osteogenic differentiation require further investigation.

Human bone tissue exhibits multi-level structures at the macro-, micro-, and nano-scale levels.[26] By creating multi-scale composite structures on the implant material surfaces, their osteogenic performance can be significantly

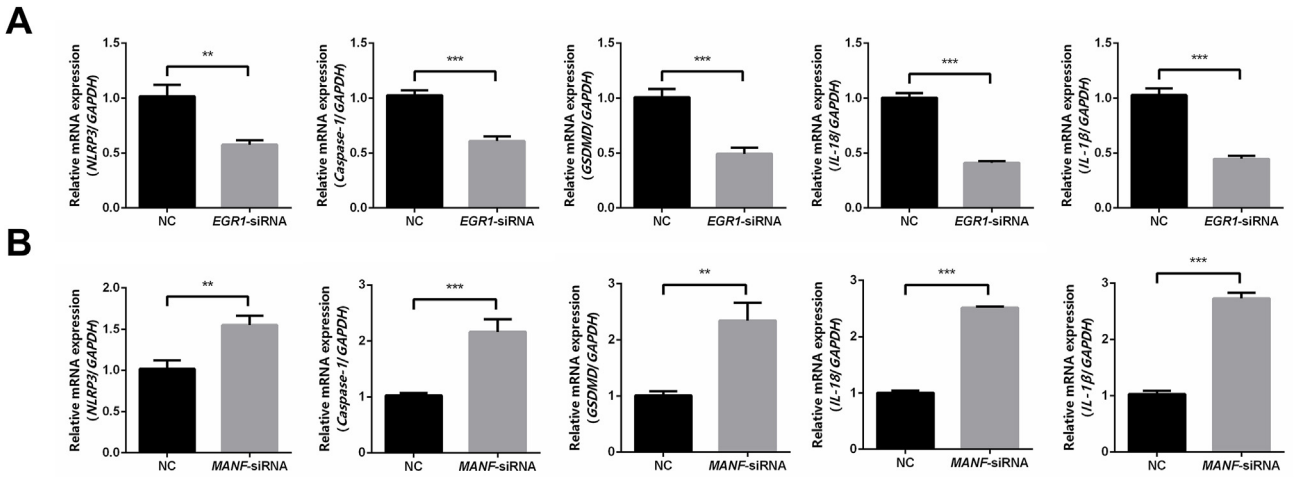

Figure 7 The mRNA expression levels of pyroptosis-associated factors after silencing key differentially expressed genes (DEGs). (A) The mRNA expression levels of pyroptosis-associated factors after silencing *EGR1*. (B) The mRNA expression levels of pyroptosis-associated factors after silencing *MANF*. Results are expressed as means ± SD, n = 3. $^{**}P < 0.01$, $^{***}P < 0.001$. EGR1: early growth response 1, GAPDH: glyceraldehyde-3-phosphate dehydrogenase, GSDMD: gasdermin D, IL: interleukin, MANF: mesencephalic astrocyte derived neurotrophic factor, NC: negative control, NLRP3: NLR family pyrin domain containing 3, siRNA: small interfering RNA.

enhanced.[22] In this study, by combining pore-forming techniques with acid etching, a micro-/nano-structured zirconia surface characterized by numerous micron-scale pores and nano-scale particles within the pores was successfully developed. Compared to the SBHF surface, this surface demonstrated a larger surface area and more pronounced micron-scale pores. The pores on the POROHF surface expanded the contact area and facilitated water penetration, thereby significantly improving hydrophilicity. XRD analysis revealed that the SLA surface consisted of amorphous titanium, lacking both anatase and rutile phases, as previously reported.[14] The combination of pore-forming technology and acid etching did not result in significant phase transitions, whereas sandblasting followed by acid etching resulted in the emergence of a distinct monoclinic phase peak on the zirconia surface, as previously reported.[27] Furthermore, to ensure adequate mechanical strength, the POROHF specimens were designed with a dense base and a porous surface. The previous research by our research group confirmed that the POROHF specimens exhibited flexural strength comparable to SBHF specimens and untreated sintered zirconia specimens.[14]

Previous researches have suggested that zirconia is associated with a reduced likelihood of inflammatory responses compared to titanium.[28] Consistent with these findings, our study demonstrated that both zirconia surfaces exhibited lower pyroptosis levels compared to the SLA surface. This reduction might be due to the differences in material composition and their effects on cellular responses under inflammatory conditions. The nano-scale rough structures present on the SBHF and POROHF surfaces, which were absent on the SLA surface, could also play a critical role in modulating pyroptosis levels.[29] Additionally, the SLA surface might contain trace amounts of titanium particles, which could enhance inflammasome activation in the presence of LPS, thereby contributing to increased pyroptosis levels under inflammatory conditions.[30]

Among the two types of zirconia surfaces, the POROHF surface exhibited lower pyroptosis levels, likely due to its more pronounced micron-scale porous structures and nanoparticles. When cells attach to a multi-scale composite surface characterized by micro-/nano-scale features, they can sense the surface topography by extending pseudopodia.[31] The micro-scale structures provide sites for cell adhesion, while the nano-scale structures modulate cellular responses to external and internal environmental changes.[31] The interaction between cells and micro-/nano-structures not only enhances osteogenesis but also influences the cellular inflammatory response.[12,32] Previous researches have shown that, compared to micro-scale SLA surfaces, titanium surfaces with micro-/nano-scale topographies can alleviate inflammatory response of macrophages and promote their polarization toward an anti-inflammatory state.[24] As demonstrated in the study, the micro-/nano-structured zirconia surface was beneficial for hBMSC adhesion, which might influence cellular inflammatory responses under inflammatory conditions by inducing cytoskeletal rearrangement. Additionally, surface wettability might play a role in modulating cellular inflammatory responses. Previous researches have found that, compared to hydrophobic surfaces, hydrophilic surfaces can promote macrophage polarization toward an anti-inflammatory state, thereby reducing inflammatory responses.[33] The POROHF surface exhibited greater hydrophilicity than the SBHF and SLA surfaces, which likely contributed to the observed reduction in pyroptosis levels. Furthermore, the POROHF surface was beneficial for hBMSC proliferation, primarily due to reduced pyroptosis and decreased expression of pro-inflammatory factors, creating a more favorable environment for cell proliferation.

Reduced inflammatory responses on material surfaces may facilitate osteogenesis under inflammatory conditions. A previous research demonstrated that a micro-/nano-structured titanium surface could alleviate the inhibitory

effects of oxidative stress on osteogenesis by enhancing oxidative resistance, thereby promoting osteogenic differentiation of BMSCs under oxidative stress conditions.[24] In this study, caspase-1/GSDMD-mediated pyroptosis was found to inhibit osteogenesis, while inhibiting pyroptosis promoted osteogenic differentiation and angiogenic potential of hBMSCs on all three types of surfaces. The reduced pyroptosis levels observed on the POROHF surface alleviated the inhibitory effects of pyroptosis on osteogenesis, thereby promoting osteogenic differentiation of hBMSCs. Moreover, the POROHF surface demonstrated superior osteogenic performance under both physiological conditions[14] and in the presence of caspase-1 inhibitor under inflammatory conditions. This highlighted the intrinsic superior osteogenic performance of the POROHF surface, which could maintain enhanced osteogenic performance even when osteogenesis was partially inhibited under inflammatory conditions. Bone regeneration and angiogenesis are intricately linked processes that mutually enhance each other.[34] Consistent with this, the levels of angiogenic-associated genes in this study mirrored the trends observed in osteogenic-associated genes on different surfaces. These findings imply that the application of the POROHF surface combined with the reduced pyroptosis levels can enhance osteogenic performance under inflammatory conditions, offering valuable insights for clinical applications.

Sequencing results, further validated by RT-qPCR, confirmed that the POROHF group exhibited lower *EGR1* expression levels and higher *MANF* expression levels compared to the SBHF and SLA groups. EGR1, a transcriptional regulator, is activated by various stimuli, such as hypoxia and oxidative stress.[35] In addition, the influence of surface topography on *EGR1* expression may occur via mechanotransduction.[36] Kim et al. reported that lysophosphatidic acid upregulated *NLRP3* expression and induced pyroptosis by increasing *EGR1* expression in podocytes,[37] implying that *EGR1* might function as an upstream of caspase-1/GSDMD-mediated pyroptosis pathway. It is speculated that the POROHF surface downregulates *EGR1* expression by mechanotransduction, thereby reducing pyroptosis. MANF, an anti-inflammatory factor, plays a protective role in non-neuronal tissues.[38] Previous researches have demonstrated that *MANF* can inhibit NF-κB activation, consequently alleviating inflammatory responses.[39] Thus, *MANF* may suppress the activation of NLRP3 by inhibiting NF-κB, contributing to the reduced pyroptosis level observed in hBMSCs on the POROHF surface. As shown in the study, the levels of pyroptosis-associated genes of hBMSCs decreased after silencing *EGR1*, while the levels of pyroptosis-associated genes increased after silencing *MANF*. Therefore, *EGR1* downregulation and *MANF* upregulation on the POROHF surface, contributed to the observed reduction in pyroptosis.

In conclusion, in this study we induced caspase-1/GSDMD-mediated pyroptosis in hBMSCs and confirmed its inhibitory effects on osteogenic differentiation and angiogenic potential of hBMSCs. Notably, inhibiting pyroptosis enhanced the osteogenic performance of material surfaces under inflammatory conditions. Compared to sandblasted and acid-etched titanium and zirconia surfaces, the micro-/nano-structured zirconia surface could reduce pyroptosis levels, thereby promoting osteogenic differentiation and angiogenic potential of hBMSCs. The surface reduced pyroptosis levels of hBMSCs by downregulating *EGR1* expression and upregulating *MANF* expression, thereby promoting osteogenesis. Considering the potential role of pyroptosis in peri-implantitis, the reduced pyroptosis levels and enhanced osteogenic performance of the material surfaces under inflammatory conditions may be beneficial in reducing the bone loss associated with peri-implantitis. Therefore, we speculate that this surface modification may contribute to the prevention and alleviation of peri-implantitis. However, further *in vivo* studies using animal models of peri-implantitis are required to confirm the osseointegration potential of micro-/nano-structured zirconia implants in the inflammatory microenvironment. Additionally, the mechanistic investigation in this study serves as a preliminary exploration, offering valuable insights but leaving room for further research. For instance, how oxidative stress influences pyroptosis and osteogenic differentiation of hBMSCs under the inflammatory conditions, as well as the specific signaling pathways through which pyroptosis inhibits the osteogenic differentiation of hBMSCs, remain to be elucidated.

Declaration of competing interest

The authors have no conflicts of interest relevant to this article.

Acknowledgments

The study was funded by the Beijing Natural Science Foundation-Haidian Original Innovation Joint Fund Project [grant number L232025], the Clinical Research Foundation of Peking University School and Hospital of Stomatology, China [grant number PKUSS-2023CRF503], and the Beijing Natural Science Foundation [grant number 7222224]. The authors thank Xinjie Liang from Zhong Xin Tang Guo Ye Medical Technology Co., Ltd. (China) for supplying the porous surface zirconia specimens.

Appendix A. Supplementary data

Supplementary data to this article can be found online at https://doi.org/10.1016/j.jds.2025.02.012.

References

1. Berglundh T, Armitage G, Araujo MG, et al. Peri-implant diseases and conditions: consensus report of workgroup 4 of the 2017 world Workshop on the Classification of periodontal and peri-implant diseases and conditions. *J Clin Periodontol* 2018; 45(Suppl 20):S286—91.
2. Diaz P, Gonzalo E, Villagra LJG, Miegimolle B, Suarez MJ. What is the prevalence of peri-implantitis? A systematic review and meta-analysis. *BMC Oral Health* 2022;22:449.
3. Wu X, Qiao S, Wang W, et al. Melatonin prevents peri-implantitis via suppression of TLR4/NF-kappaB. *Acta Biomater* 2021;134:325—36.
4. Shi JJ, Zhao Y, Wang K, et al. Cleavage of GSDMD by inflammatory caspases determines pyroptotic cell death. *Nature* 2015;526:660—5.

5. Li XY, Ji L, Men X, et al. Pyroptosis in bone loss. *Apoptosis* 2023;28:293—312.
6. Zhang RN, Sun ZJ, Zhang L. Pyroptosis in inflammatory bone diseases: molecular insights and targeting strategies. *FASEB J* 2022;36:e22670.
7. Chen CZ, Jiang ZW, Jiang QF, et al. Caspase-3 and gasdermin E detection in peri-implantitis. *Acta Mol Basis Dis* 2021;1867: 166217.
8. Chen LW, Tang ZQ, Fu LL, et al. The critical role of pyroptosis in peri-implantitis. *J Inflamm Res* 2024;17:1621—42.
9. Xu Y, Shen Z, Zhou Y, et al. Osteogenic and anti-inflammatory effects of SLA titanium substrates doped with chitosan-stabilized selenium nanoparticles via a covalent coupling strategy. *Colloids Surf B Biointerfaces* 2023;224:113217.
10. Sivaraman K, Chopra A, Narayan AI, Balakrishnan D. Is zirconia a viable alternative to titanium for oral implant? A critical review. *J Prosthodont Res* 2018;62:121—33.
11. Haugen HJ, Chen HY. Is there a better biomaterial for dental implants than titanium?-A review and meta-study analysis. *J Funct Biomater* 2022;13:46.
12. Liu Y, Rui Z, Cheng W, et al. Characterization and evaluation of a femtosecond laser-induced osseointegration and an anti-inflammatory structure generated on a titanium alloy. *Regen Biomater* 2021;8:rbab006.
13. Zhou Y, Tang CZ, Deng JL, Xu RG, Yang Y, Deng FL. Micro/nano topography of selective laser melting titanium inhibits osteoclastogenesis via mediation of macrophage polarization. *Biochem Biophys Res Commun* 2021;581:53—9.
14. Gao Y, Ding Q, Li WJ, Gu RL, Zhang P, Zhang L. Role and mechanism of a micro-/nano-structured porous zirconia surface in regulating the biological behavior of bone marrow mesenchymal stem cells. *ACS Appl Mater Interfaces* 2023;15:14019—32.
15. Toraya H, Yoshimura M, Somiya S. Calibration curve for quantitative analysis of the monoclinic-tetragonal ZrO2 system by X-ray diffraction. *J Am Ceram Soc* 1984;67. C-119-21.
16. Garvie RC, Nicholson PS. Phase analysis in zirconia systems. *J Am Ceram Soc* 2006;55:303—5.
17. Lv XF, Fan C, Jiang ZX, Wang WX, Qiu X, Ji QX. Isoliquiritigenin alleviates P. gingivalis-LPS/ATP-induced pyroptosis by inhibiting NF-κB/NLRP3/GSDMD signals in human gingival fibroblasts. *Int Immunopharmacol* 2021;101:108338.
18. Tang YS, Zhao YH, Zhong Y, et al. Neferine inhibits LPS-ATP-induced endothelial cell pyroptosis via regulation of ROS/NLRP3/Caspase-1 signaling pathway. *Inflamm Res* 2019;68: 727—38.
19. Wang L, Dong XB, Feng SY, et al. VX765 alleviates dextran sulfate sodium-induced colitis in mice by suppressing caspase-1-mediated pyroptosis. *Int Immunopharmacol* 2022;102:108405.
20. Withanage MHH, Liang H, Zeng E. RNA-seq experiment and data analysis. *Methods Mol Biol* 2022;2418:405—24.
21. Sun J, Ding Q, Chen Y, et al. Effects and underlying mechanism of micro-nano-structured zirconia surfaces on biological behaviors of human gingival fibroblasts under inflammatory conditions. *Acta Biomater* 2024;183:356—70.
22. Kligman S, Ren Z, Chung CH, et al. The impact of dental implant surface modifications on osseointegration and biofilm formation. *J Clin Med* 2021;10:1641.
23. Xiong SB, Lu XG, Zhang SQ, et al. Osteogenic properties of bioactive titanium in inflammatory environment. *Dent Mater* 2023;39:929—37.
24. Huang J, Li R, Yang J, et al. Bioadaptation of implants to in vitro and in vivo oxidative stress pat hological conditions via nanotopography-induced FoxO1 signaling pathways to enhance osteoimmunal regeneration. *Bioact Mater* 2021;6:3164—76.
25. Xu XH, Zhang TW, Xia XY, et al. Pyroptosis in periodontitis: from the intricate interaction with apoptosis, NETosis, and necroptosis to the therapeutic prospects. *Front Cell Infect Microbiol* 2022;12:953277.
26. Coelho PG, Jimbo R, Tovar N, Bonfante EA. Osseointegration: hierarchical designing encompassing the macrometer, micrometer, and nanometer length scales. *Dent Mater* 2015;31: 37—52.
27. Ding Q, Zhang L, Bao R, Zheng G, Sun YC, Xie QF. Effects of different surface treatments on the cyclic fatigue strength of one-piece CAD/CAM zirconia implants. *J Mech Behav Biomed Mater* 2018;84:249—57.
28. Moura Neto J, Cardoso LM, Pansani TN, Raucci LMSC, de Souza Costa CA, Basso FG. Influence of titanium and zirconia substrates on the synthesis of inflammatory mediators. *Biointerphases* 2023;18:041002.
29. Andrukhov O, Behm C, Blufstein A, et al. Effect of implant surface material and roughness to the susceptibility of primary gingival fibroblasts to inflammatory stimuli. *Dent Mater* 2020; 36:e194—205.
30. Insua A, Galindo-Moreno P, Miron RJ, Wang HL, Monje A. Emerging factors affecting peri-implant bone metabolism. *Periodontol 2000* 2024;94:27—78.
31. Ji ZB, Wan Y, Wang HW, et al. Effects of surface morphology and composition of titanium implants on osteogenesis and inflammatory responses: a review. *Biomed Mater* 2023;18: 042002.
32. He YD, Li Z, Ding X, et al. Nanoporous titanium implant surface promotes osteogenesis by suppressing osteoclastogenesis via integrin β1/FAKpY397/MAPK pathway. *Bioact Mater* 2022;8: 109—23.
33. Hotchkiss KM, Reddy GB, Hyzy SL, Schwartz Z, Boyan BD, Olivares-Navarrete R. Titanium surface characteristics, including topography and wettability, alter macrophage activation. *Acta Biomater* 2016;31:425—34.
34. Zheng S, Zhou CH, Yang H, et al. Melatonin accelerates osteoporotic bone defect repair by promoting osteogenesis-angiogenesis coupling. *Front Endocrinol* 2022;13:826660.
35. Woodson CM, Kehn-Hall K. Examining the role of EGR1 during viral infections. *Front Microbiol* 2022;13:1020220.
36. Vermeulen S, Roumans N, Honig F, et al. Mechanotransduction is a context-dependent activator of TGF-β signaling in mesenchymal stem cells. *Biomaterials* 2020;259:120331.
37. Kim D, Ban KY, Lee GH, Jun HS. Lysophosphatidic acid induces podocyte pyroptosis in diabetic nephropathy by an increase of Egr1 expression via downregulation of EzH2. *Int J Mol Sci* 2023; 24:9968.
38. Liu YY, Huo D, Zeng LT, et al. Mesencephalic astrocyte-derived neurotrophic factor (MANF): structure, functions and therapeutic potential. *Ageing Res Rev* 2022;82:101763.
39. Wang CH, Bao Q, Hou C, et al. Mono-macrophage-derived MANF alleviates bacterial myocarditis by inhibiting NF-kappaB activation and myocardial inflammation. *Inflammation* 2021;44: 1916—26.